Protein Science (1994), *3*:188-197. Cambridge University Press. Printed in the USA.

Structure and dynamics of the active site gorge of acetylcholinesterase: Synergistic use of molecular dynamics simulation and X-ray crystallography

PAUL H. AXELSEN,[1,2] MICHAL HAREL,[2] ISRAEL SILMAN,[3] AND JOEL L. SUSSMAN[2]

[1] Department of Pharmacology, University of Pennsylvania, Philadelphia, Pennsylvania 19104
[2] Department of Structural Biology, Weizmann Institute of Science, Rehovot 76100, Israel
[3] Department of Neurobiology, Weizmann Institute of Science, Rehovot 76100, Israel

(RECEIVED July 30, 1993; ACCEPTED November 30, 1993)

Abstract

The active site of acetylcholinesterase (AChE) from *Torpedo californica* is located 20 Å from the enzyme surface at the bottom of a narrow gorge. To understand the role of this gorge in the function of AChE, we have studied simulations of its molecular dynamics. When simulations were conducted with pure water filling the gorge, residues in the vicinity of the active site deviated quickly and markedly from the crystal structure. Further study of the original crystallographic data suggests that a bis-quaternary decamethonium (DECA) ion, acquired during enzyme purification, resides in the gorge. There is additional electron density within the gorge that may represent small bound cations. When DECA and 2 cations are placed within the gorge, the simulation and the crystal structure are dramatically reconciled. The small cations, more so than DECA, appear to stabilize part of the gorge wall through electrostatic interactions. This part of the gorge wall is relatively thin and may regulate substrate, product, and water movement through the active site.

Keywords: decamethonium; molecular dynamics simulation; quaternary ammonium compounds; serine hydrolase; solvation; X-ray crystallography

Acetylcholinesterase (AChE) catalyzes the hydrolysis of acetylcholine (ACh^+) into acetate and choline at cholinergic nerve terminals. It is an extremely effective catalyst, acting at nearly diffusion-controlled rates to terminate the action of ACh on postsynaptic receptors (Quinn, 1987). It is, therefore, remarkable that the active site of this enzyme is found at the bottom of a deep and narrow gorge (Sussman et al., 1991). We do not yet know whether this gorge provides a mechanism that somehow facilitates the rapid action of the enzyme, or whether it has an altogether different role, and the enzyme is able to operate rapidly in spite of impeded access of substrate to the active site.

The gorge has 2 remarkable structural features that may hint at its role. First, the walls of the gorge are lined predominantly by aromatic residue side chains. Quaternary ammonium ions do not bind to an anionic subsite as once supposed (Nachmansohn & Wilson, 1951); instead, they interact directly with the aromatic side chains of Trp 84, Phe 330, and Trp 279 (Harel et al., 1993). Second, the overall distribution of charged residues in AChE gives rise to a large electrostatic dipole that is precisely aligned with the gorge axis. The field due to this dipole will draw positively charged substrates toward and down the gorge to the active site (Ripoll et al., 1993; Tan et al., 1993). It has been suggested that these 2 features may work together, like an affinity electrophoresis column, with the dipole providing motive force and the aromatic groups providing a series of low-affinity binding sites for quaternary ions (Sussman & Silman, 1992; Ripoll et al., 1993).

Beyond these startling revelations, crystallography has not further clarified the functional implications of the gorge or of the aromatic residues that form its surface. One reason for this is that crystallography does not yield unequivocal information about the contents of the gorge. The solvent and ion content of the gorge may have considerable influence on the electrostatic properties of the enzyme and upon the forces within the gorge that determine the bound conformation of various ligands. A second reason is that crystallography yields only limited information about structural dynamics (Ringe & Petsko, 1985). The movement of ligands in and out of the active site will be restricted both by the narrow dimensions of the gorge and by the presence of solvent within. These considerations necessitate some kind of conformational change in the gorge walls akin to "breathing" and/or the existence of a "back door" (Ripoll et al., 1993) for the escape of solvent and reaction products.

To better understand the function of the active site gorge, a detailed description of its dynamic topography is clearly necessary. In the following, we present 2 approaches to this descrip-

Reprint requests to: Paul H. Axelsen, Department of Pharmacology, University of Pennsylvania, Philadelphia, Pennsylvania 19104-6084; e-mail: axe@pharm.med.upenn.edu.

tion and demonstrate their potential for synergistic application: (1) a crystallographic approach, using data sets collected for the native enzyme and for several enzyme–ligand complexes, and (2) a computational approach, using molecular dynamics simulation to develop a dynamic model of the gorge.

Results

Structure

AChE is roughly an ellipsoid featuring a catalytic triad of residues Ser 200, His 440, and Glu 327 near the base of a narrow cavity approximately 20 Å deep (Kinemage 1). Crystallographic studies aimed at elucidating structure–function relationships in the active site have employed the conventional approach of soaking suitable ligands into the protein crystal. This has now been successful for several anticholinesterase agents of pharmacological interest (Table 1). Ligand–enzyme complexes isomorphous with the native structure have been obtained in each case, thus permitting ready structure determination (Harel et al., 1993; M. Harel, I. Silman, & J.L. Sussman, unpubl.).

Considering the ease with which ligands could be exchanged in the crystalline enzyme, it was surprising to discover that the opening of the active site gorge is tightly capped by a symmetry-related copy of the enzyme (Fig. 1). The copy is related by a 3-fold screw axis about z $(1-y, 1+x-y, z+1/3)$. With only 1 molecule in the asymmetric unit, the gorge opening of every enzyme molecule in the crystal is similarly capped. The interaction between the gorge rim and the symmetry-related molecule involves at least 5 ion pairs (Glu 73–Lys 192, Lys 107–Asp 276, Lys 11–Asp 285, Asp 217–Lys 341, and Arg 216–Asp 342). Although we find 2 sinuous routes from the gorge interior to the protein exterior, they are narrow and only large enough for a single water molecule.

We used information about the crystal symmetry to define the gorge volume. A model of an AChE monomer and of the symmetry-related copy that blocks its gorge opening was immersed in solvent water molecules (see description of the solvated dynamics simulation below). The CHARMM "search" utility, which locates unoccupied "vacuum" points on a 3-dimensional grid, was applied to this model after a set of contiguous water molecules within the gorge had been deleted. The utility provides coordinates for each vacuum point found so that the cavity that corresponds to the calculated volume can be visually examined. Using an extended radius of 1.4 Å for each protein atom and a grid spacing of 0.1 Å, this method yields a volume of 313 Å^3.

Table 1. *Crystallographic data for AChE–ligand complexes*

Identifier[a]	Ligand	Cell dimensions $a = b$	Cell dimensions c	R-factor[b]
1ACE	[c]	112.8	137.0	0.213
DECA	Decamethonium	113.05	137.5	0.223
EDR	Edrophonium	113.3	137.7	0.210
THA	Tacrine	113.7	138.1	0.212
IP	[c]	113.54	137.91	0.236
Hg	Mercury (II)[c]	110.7	135.0	0.220
U	Uranium (III)[c]	110.88	134.67	0.222
Xrt	[c]	110.55	135.09	0.216

[a] The 1ACE structure was deposited in the Brookhaven Protein Data Bank and was derived from data collected at 0 °C on a Siemens/Xentronics area detector. All other data sets were collected at room temperature. 1ACE, IP, and Xrt are data sets derived from similarly prepared crystals but with different instrumentation or temperature (IP: RAXIS-II image plate at room temperature; Xrt: Siemens/Xentronics area detector at room temperature).

[b] The R-factors listed were those after "preliminary" refinement starting from the 1ACE coordinates without including solvent or DECA molecules (see Methods for details).

[c] As discussed in the text, these structures appear to contain a molecule of DECA in the active site gorge.

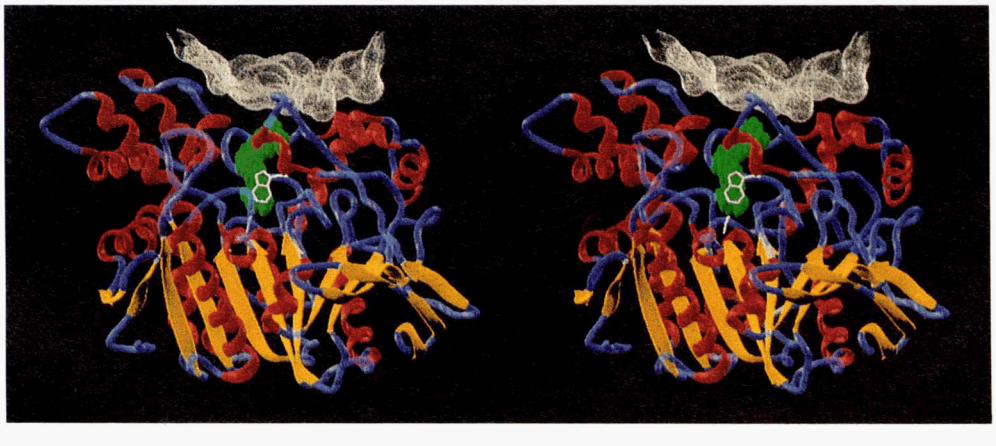

Fig. 1. Ribbon diagram of AChE. Helix, sheet, and coil segments are shown in red, yellow, and blue, respectively. Residues 485–489, which were not seen in the electron density map, are shown as a break in the coil at the lower right. A molecule of DECA (green) is included to indicate the location of the gorge. Ser 200 and Trp 84 are shown in white stick figures to indicate the location of the active site and an especially thin portion of the gorge wall, respectively. A Connolly dot surface (Connolly, 1983) of a portion of the symmetry-related copy of the enzyme is shown to illustrate how the gorge opening (in the top and middle of the ribbon figure) is capped. Image generated using RIBBONS by M. Carson.

The gorge is approximately 20 Å deep and has an irregular cross section (Fig. 2; Kinemages 1, 2). If approximated as a cylinder, the gorge would have an average diameter of 4.4 Å. This compares to 6.4 Å for the van der Waals (VDW) diameter of a tetramethylammonium ion. Since this approximates the largest cross section of an ACh molecule, ACh and other quaternary ammonium ligands are too large to enter and leave the active site through the gorge as seen in the X-ray structure. For this reason, the possible existence of a "back door," already alluded to above (Ripoll et al., 1993), bears consideration as an alternate route for ligand entry into the active site. To do so requires examining the structure of the gorge with a particular view toward defining possible alternative access routes to the active site.

Roughly 3/4 of the gorge wall is 2 or more residues thick, while 1/4 is relatively thin, i.e., only 1 residue thick (Fig. 3). The thin aspect of the gorge wall is comprised entirely of the segment of residues between Cys 67 and Cys 94, which are disulfide-linked. Within this segment, residues 79–83 may be considered as 1 turn of an α-helix, and residues 82–85 form a distorted β-turn of indeterminate type. Aside from these, an omega loop (Leszczynski & Rose, 1986) is the only secondary structure descriptor that applies to residues 67–94. Residues comprising the

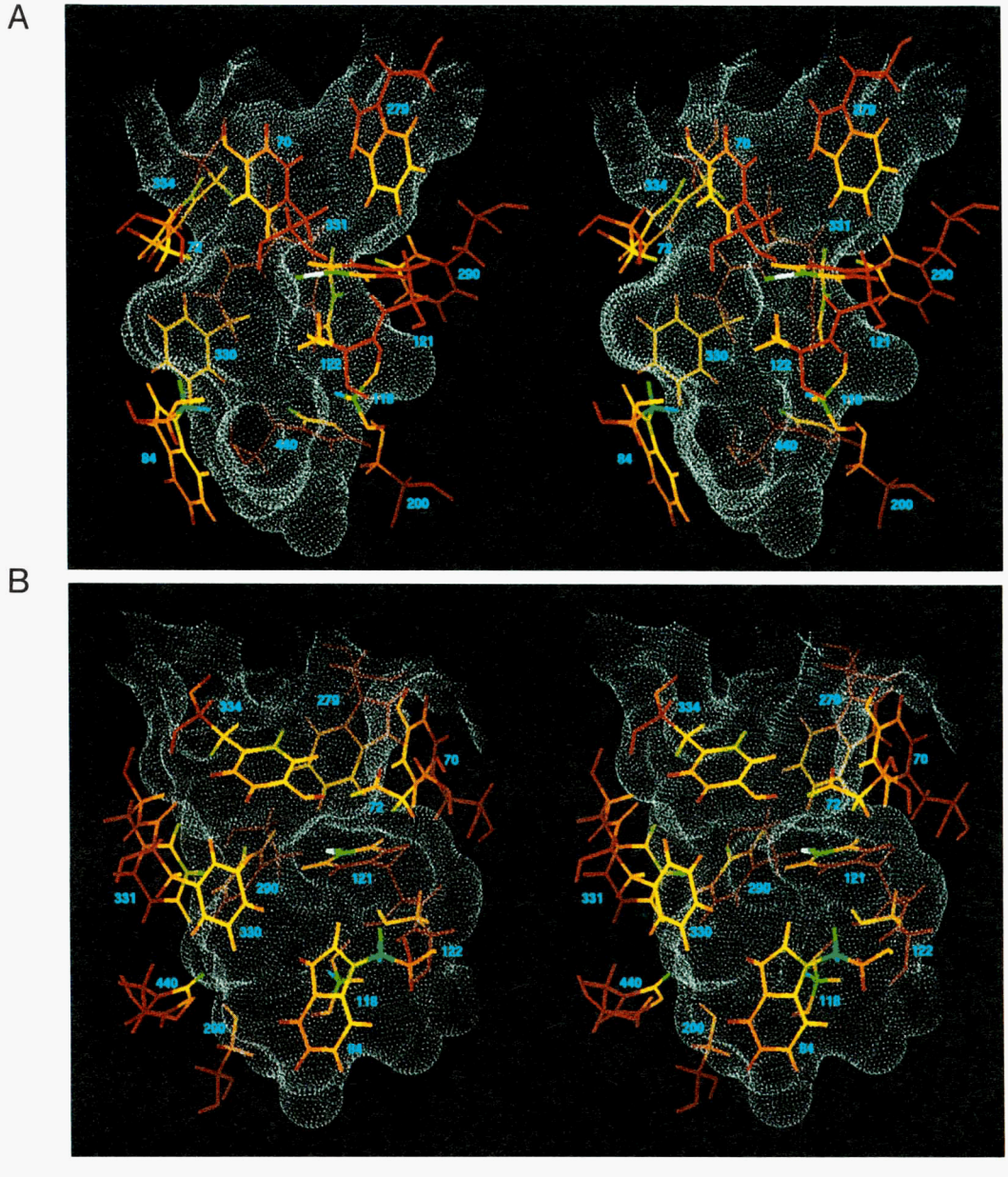

Fig. 2. Residues comprising the gorge wall. The Connolly dot surface (white) was generated with a 1.6-Å-radius probe, and atoms are color-coded according to their fractional exposure, calculated by the method of Lee and Richards (1971) within CHARMM. Color order: green = maximally exposed, white, yellow, orange, red = not exposed. Panels **A** and **B** are rotated approximately 90°. Image generated using QUANTA (Molecular Simulations, Inc., Burlington, Massachusetts).

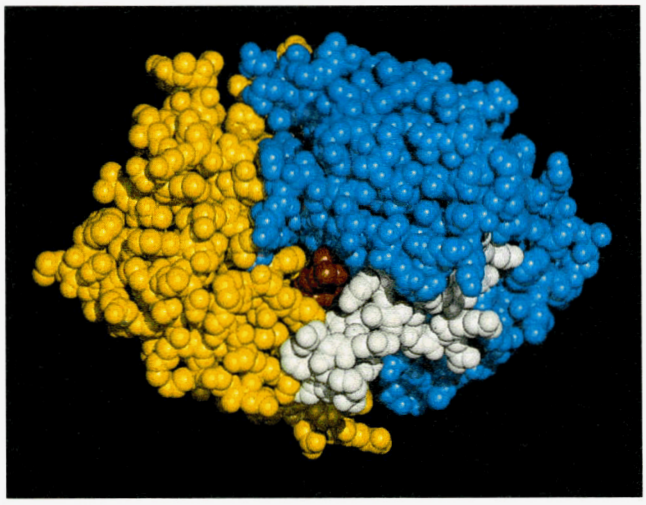

Fig. 3. Ray-trace image of the gorge opening viewed directly down the gorge axis. N-terminal residues 4–310 are in blue, except for 67–94 (white), which represent the thin wall. Residues 311–534 are in yellow, and a molecule of DECA in the gorge is in red. Image generated with QUANTA.

thicker portions of the gorge wall participate in 2 short helices (residues 271–278 and 328–335), but do not otherwise exhibit regular secondary structure.

Distance matrix analysis (not shown) and an examination of computer graphics models suggest that the active site gorge is formed at the interface between 2 distinct domains (Fig. 3; Kinemage 1; G. Zaccai, pers. comm.). There is an abundance of β secondary structure within each domain, though very little spans the interdomain interface. There are numerous favorable electrostatic interactions within each domain, but virtually no such interactions are found between the domains.

Using the model mentioned above, in which water molecules within the gorge had been deleted, we found the gorge walls to have a surface area of 245.7 Å^2. As previously reported (Sussman et al., 1991), these walls are largely comprised of aromatic amino acid side chains (Kinemage 2). Specifically, these aromatic side chains comprise 167.5 Å^2 or 68% of the gorge wall surface, while aliphatic side chains comprise only 1.3 Å^2 (Table 2). Using CHARMM-assigned partial charges (q_i) and fractional exposures determined in the course of computing the gorge volume above (f_i), we have calculated $\sum q_i f_i$ for the atoms in each residue lining the gorge as a rough measure of the surface polarity. This sum reflects the forces that operate in dynamics simulations and is useful in identifying which residues imbue polar character to the gorge walls. For all residues lining the gorge, the sum is $-0.443e$ ($0.072e$ positive, $0.515e$ negative). Main chain atoms including entire glycine residues contribute only $-0.019e$ ($0.064e$ positive, $0.083e$ negative). The acidic side chains of D72 and E199 contribute only $-0.112e$. Most of the negative surface potential, $-0.270e$, is due to aromatic residues, chiefly Tyr. Thus, the aromatic side chains that dominate the surface area of the gorge also dominate the electrostatic character of its surface.

Dynamics

The results of our analyses of the static AChE structure indicate that ligands may gain access to the active site only if ma-

Table 2. *Composition and electrostatic character of the active site gorge surface in AChE*[a]

Main chain				Side chain			
Residue name	Residue number	$\sum q_i f_i$	Surface area	Residue name	Residue number	$\sum q_i f_i$	Surface area
Tyr	70	−0.007	0.48	Tyr	70	−0.027	8.80
Trp	84	−0.010	1.35	Asp	72	−0.070	13.86
Asn	85	0.000	0.04	Trp	84	−0.036	34.10
Gly	117	−0.002	4.15	Asn	85	−0.010	1.06
Gly	118	0.024	18.27	Tyr	121	−0.100	38.92
Gly	119	−0.011	1.04	Ser	122	−0.008	7.49
Gly	123	−0.002	0.56	Leu	127	0.000	0.08
Ser	286	−0.014	1.19	Tyr	130	−0.014	0.49
Ile	287	0.024	1.62	Glu	199	−0.042	4.26
Phe	288	0.004	2.32	Ser	200	−0.012	2.22
Arg	289	−0.020	3.55	Trp	279	−0.033	13.92
Phe	330	−0.004	0.86	Leu	282	−0.001	0.15
Phe	331	0.001	0.44	Ile	287	−0.001	1.06
Tyr	334	0.006	0.51	Phe	290	0.007	6.25
Gly	335	−0.004	0.24	Phe	330	−0.029	17.24
His	440	−0.009	0.18	Phe	331	0.001	22.58
Gly	441	0.005	1.02	Tyr	334	−0.031	25.21
				His	440	−0.015	11.18
Overall sum		−0.019	36.81			−0.424	208.86

[a] The sums, $\sum q_i f_i$, are in units of atomic charge units (e); surface areas are in Å^2.

jor conformational changes occur among the residues that define the shape of the gorge. As an experimental means of examining the dynamics of the overall AChE structure, and in particular the dynamics of the aromatic gorge, we performed a comparative study of 8 different crystal structures. These were obtained from X-ray data collected for "native" AChE at different temperatures and using different instruments, as well as for heavy atom derivatives and ligand–AChE complexes (Table 1). In order to compare these structures in a uniform and consistent manner, preliminary crystallographic refinements were performed using the "slow cooling" protocol of X-PLOR (Brünger, 1990), as described previously (Sussman et al., 1991), starting from the 1ACE structure. All $F_o > 0\sigma$ for 6–2.8 Å resolution were used in the refinement, and all $F_o > 0\sigma$ for 20–2.8 Å resolution were used to prepare $F_o - F_c$ difference Fourier maps. Water and ligands were not included in this preliminary refinement, nor was there any manual refitting of the structural changes to the maps.

Although slow cooling can induce large changes, we found that all 8 crystal structures retain the same basic conformation. A comparison of RMS differences after least-squares fitting of the main chain atoms is given in Figure 4. It should be emphasized that the structure of the active site and the gorge walls remains essentially constant in the presence or absence of quite different ligands. In particular, this is true for the "omega loop," residues 67–94. As mentioned above, these residues comprise the thin aspect of the gorge wall; they have relatively little interaction with other parts of the protein and virtually no regular secondary structure. Thus, the interactions that stabilize this "omega loop" are not immediately evident.

In light of the results from this set of X-ray structures, we prepared a molecular dynamics simulation designed specifically to examine the dynamics of the gorge walls (see Methods). We included the symmetry-related molecule that blocks the gorge orifice for 2 reasons: (1) we sought to understand the interactions that stabilize the thin wall of the gorge (the top edge of this wall makes multiple steric contacts with the symmetry-related copy), and (2) we sought information about how ligands gain access to the active site in the crystal, i.e., with the gorge blocked.

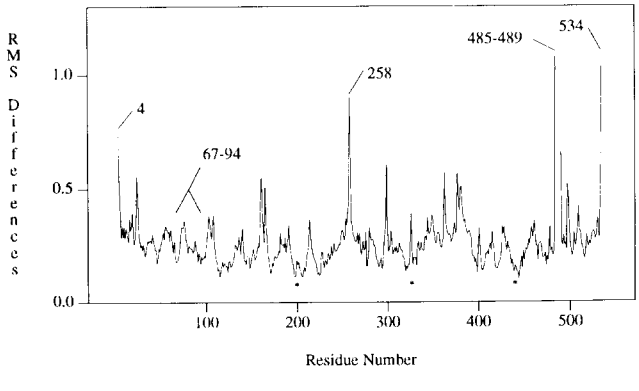

Fig. 4. RMS fluctuations around their average coordinates for the 8 crystal structures listed in Table 1. Residues 4, 484, 490, and 534 are adjacent to disordered regions of the crystal structure and therefore have relatively large differences. Ser 258 is on the surface and distant from the gorge. Residues 67–94 comprise the "omega loop" that forms the thin wall of the gorge. The 3 asterisks indicate active site triad residues Ser 200, Glu 327, and His 440.

Initial results from this simulation showed that general features of the crystal structure were retained for over 150 ps; however, residues in the vicinity of the active site triad (Ser 200, Glu 327, His 440) deviated sharply and persistently from the starting crystal structure. Specifically, the main chains of His 440 and Gly 441 translated over 2 Å, the χ_1 and χ_2 dihedral angles of His 440 rotated by 180°, and the plane of the His 440 ring tilted almost 90° from that in the crystal structure. In addition, anomalous behavior also occurred in residues 82–85. This segment forms a somewhat distorted β-turn, and it includes Trp 84, which has an important role in quaternary ligand binding (Weise et al., 1990; Harel et al., 1993). Within 3–4 ps of beginning the simulation, the hydrogen bond between 82:O and 85:HN is broken, and all resemblance to a β-turn is lost.

Because these portions of the structure distorted more quickly and more radically than any other, we initially questioned the accuracy of the crystal structure in this area. However, after examining omit maps and the quality of the fit, we concluded that there was no other reasonable fit. Further examination of the simulation indicated that the β-turn was unfolding because of a VDW collision between atom 82:O and the H_β atoms of residue 85. Because the coordinates were refined using X-PLOR with a polar hydrogen parameter set that does not explicitly model H_β atoms, we reformatted the parameter set used in CHARMM for use in X-PLOR and repeated the structure refinement. However, this changed neither the structure nor the behavior of residues 82–85.

Next, we considered whether it might be necessary to incorporate solutes of the crystallizing liquor into the simulation in order for the simulation to faithfully retain the 3D relationships among residues in the active site as found in the crystal. Because this liquor was equilibrated with 61% saturated $(NH_4)_2SO_4$, we conducted a simulation with NH_4^+, SO_4^{2-}, and H_2O in a mole ratio of 2:1:5 in the solvent region external to the gorge. We also sought to determine whether SO_4^{2-} had a conspicuous affinity for any sites on the molecular surface that could be corroborated by the X-ray data. The results indicated that the solute had no effect on the β-turn involving residues 82–85 nor on the overall structure. The only site for which SO_4^{2-} had a demonstrable affinity was a lysine side chain that was not seen in the X-ray data.

Finally, a search for electron density peaks in an $F_o - F_c$ difference Fourier map of the native structure was made to identify any unaccounted for density, both internal and external to the gorge, that might be influencing the behavior of residues 82–85. For this purpose, an electron density map was prepared that included low-resolution data from 20.0 to 2.8 Å (original refinements and maps were prepared using only 8.0–2.8-Å data). It was apparent from this map, more so than from the map prepared from only 8.0–2.8-Å data, that several of the peaks that had been assigned earlier to waters in the gorge were interconnected, with electron density at least $\sigma = 3.5$ above background. Other peaks within the gorge, and presumed to be water, remained more or less discrete (Fig. 5). The dimensions and shape of the interconnected strand immediately suggested that it represented something other than water. Recalling that (1) DECA is used in the purification process to elute AChE from an affinity column (Sussman et al., 1988), (2) attempts to soak DECA into these crystals yielded maps that were virtually indistinguishable from the original map (Harel et al., 1993), and (3) other large ligands were readily seen in the gorge in experiments in

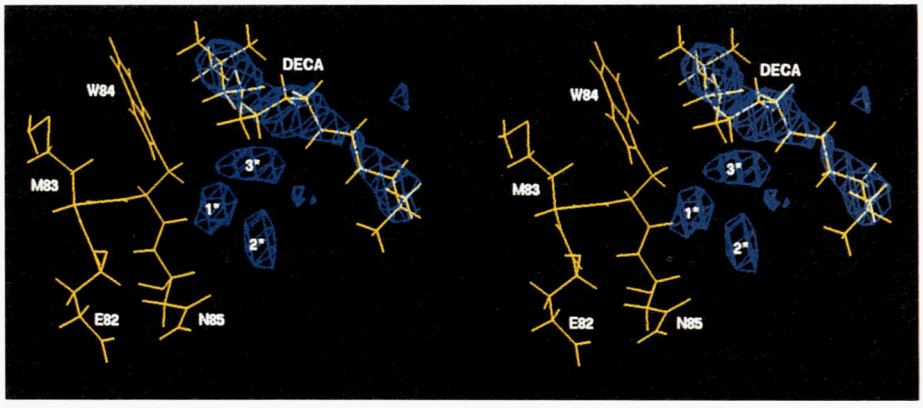

Fig. 5. Electron density map ($F_o - F_c$) map at 20–2.8 Å resolution contoured at 3.5σ generated from the observed 1ACE X-ray structure after preliminary refinement using only the protein coordinates (see Methods). Resides 82–84 are shown with a molecule of DECA fitted to the elongated density found in the gorge. The 3 highest peaks of electron density that are within the gorge, but not accounted for by DECA, are indicated as 1*, 2*, and 3* in order of decreasing peak electron density. Image generated using TOM by C. Cambillau and A. Chirino.

which they had been soaked in, we hypothesized that DECA was present in the original native crystals from which the 1ACE structure was derived. We found that a model of DECA fits very well into the elongated density (Fig. 5) and that the *R*-factor improves from 21.3 to 20.3% when a DECA molecule (but no water molecules) is included in the refinement.

Simulations were then conducted as before except that the starting structure now included 1 molecule of DECA within the gorge. This did not improve the overall agreement between simulation and crystal structure (Fig. 6A), nor did it help reconcile the conformation of the active site triad side chains (Fig. 6B). We therefore considered the possibility that 3 discrete peaks of electron density near the bottom of the gorge (Fig. 5), previously refined as water molecules, might instead be positively charged ions. We shall refer below to peaks 1 (5.7σ), 2 (5.6σ), and 3 (5.5σ) in order of decreasing electron density (Fig. 5). These peaks correspond to water molecules 23, 31, and 17, respectively, in the 1ACE crystal structure, and they are the 3 largest peaks in the gorge not accounted for by protein or DECA atoms. There are several protein moieties in the vicinity of each peak that might stabilize a cation: the carbonyl oxygen of Ser 81 and the polar side chains of Asp 72 and Tyr 334 in the case of peak 1; the carbonyl oxygens of Tyr 70 and Trp 84 and the polar side chains of Asn 85, Gln 89, and Ser 122 in the case of peak 2; the carbonyl oxygens of Gly 117 and Ser 122 and the polar side chains of Ser 122 and Tyr 130 in the case of peak 3. In addition, each peak is adjacent to a cavity large enough for 1 or 2 water molecules; these may also help to stabilize a cation.

Although all crystallographically defined waters were included in the original simulation without DECA, we omitted these waters in our initial refinement of AChE with DECA in the gorge. In the course of overlaying bulk solvent onto the crystal structure, a water molecule is placed at each of the aforementioned peaks of electron density. This is fortuitous, since no positional information about electron density is given to CHARMM as input, yet it shows that failure of the simulation to retain the crystal structure is not due to the omission of crystal waters at these sites in the starting structure. The obvious candidate for a bound cation would be NH_4^+, because its concentration in the mother liquor is over 4 M, and NH_4^+ would be crystallographically indistinguishable from water at the present crystallographic resolution (2.8 Å). Accordingly, we repeated the simulation substituting an NH_4^+ ion for each of the 3 assumed waters in these sites.

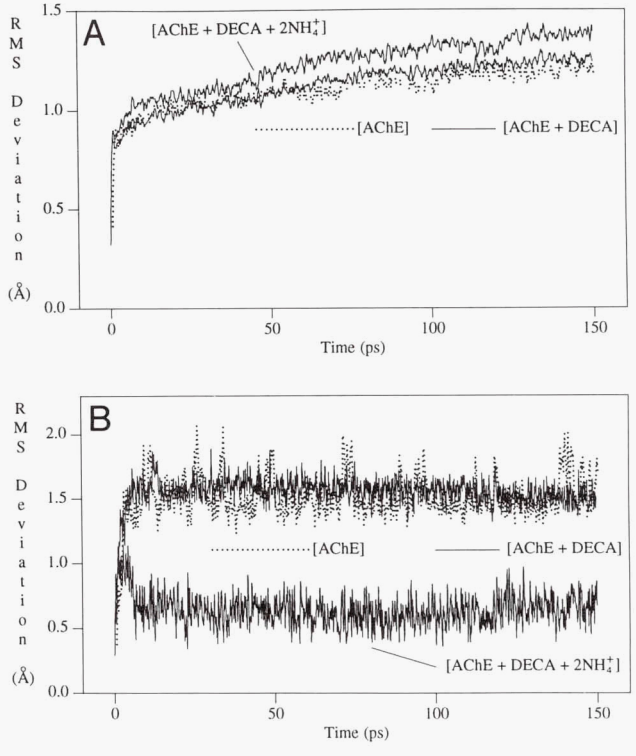

Fig. 6. RMS deviation from the starting (crystal) structure versus time for 3 different molecular dynamics trajectories. [AChE] includes only water in the gorge. [AChE + DECA] has 1 molecule of decamethonium^{2+} and several waters in the gorge. [AChE + DECA + 2NH_4^+] is the same as [AChE + DECA] but with 2 NH_4^+ ions substituting for 2 waters. All 3 simulations used selected coordinates from 1ACE and a symmetry-related copy for a starting structure. **A:** All unconstrained non-hydrogen atoms. **B:** Non-hydrogen atoms in the side chains of Ser 200, Glu 327, and His 440.

The substitution of an ammonium ion for any single water peak did not correct the side chain conformations of the active site triad residues. However, substituting ammonium ions for water at both peaks 1 and 2 had several salutary effects. (1) The RMS difference between the simulation and the crystal structure for the triad side chains decreased from 1.6 Å to 0.7 Å (Fig. 6B). (2) The average position of the active site triad side

chains over the last 75 ps of the simulation virtually coincided with the starting crystal structure (not shown), indicating that the RMS difference of 0.7 Å reflects fluctuations about the crystal structure mean. This difference corresponds to a temperature factor of 12.3 $Å^2$, nearly the same mean temperature factor as for the triad side chains in the 1ACE structure (12.7 $Å^2$). (3) The donor-acceptor distance between atoms Glu 82:O and Asn 85:N decreased from over 6 Å to between 4 and 5 Å, with frequent excursions to the crystal structure distance of 2.9 Å (data not shown). These effects were not observed if ammonium ions were placed at peaks 1 and 3 or at peaks 2 and 3.

There is an interesting consequence of substituting ammonium ions for water at all 3 peaks. Within 20 ps of beginning the simulation, the ion at peak 3 causes the side chain of Trp 84 to rotate dramatically, the ion itself migrates to the base of the gorge, and the ion at peak 2 penetrates the gorge wall and escapes to the solvent. This is accompanied by a variety of other changes in the 67-94 loop and by marked conformational departures from the crystal structure.

We performed the following control simulations to test the conclusion that 2 ammonium ions are present in the 1ACE crystal structure. The first 40 ps of the simulation with DECA and 2 ammonium ions was repeated on a different computer (an SGI 4D/240). These results, when plotted as in Figure 6, were indistinguishable from the simulation performed on a Cray YMP. Two 20-ps simulations were also repeated with altered partial charges on the ammonium ions. Irrespective of whether the charges were zeroed at the beginning of the simulation or after 10 ps of simulation with normal charges, the simulations began to behave like the AChE + DECA simulation within 5 ps. Thus, the charge of the ammonium ions is the essential characteristic that corrects the simulation, not their size or shape.

Finally, we tested the ability of the simulations to distinguish between NH_4^+ and Na^+ ions by substituting Na^+ ions for peaks 1 and 2. The CHARMM model of a sodium ion had a VDW radius of 1.65 Å, which was similar to that of 1.85 Å for NH_4^+. However, the unit charge for Na^+ was spherically uniform, whereas the nitrogen of NH_4^+ bore a partial charge of $-0.4e$ and each hydrogen had $+0.35e$. In a 50-ps simulation, we found the behavior of a simulation with 2 Na^+ ions to be indistinguishable from the simulation with 2 NH_4^+ ions. Thus, while these ions clearly had distinct chemical behavior, and even though they were modeled somewhat differently by CHARMM, we have not yet found a basis by which to distinguish between these 2 ions using simulations.

Discussion

In this study, we have used molecular dynamics simulation to advance our understanding of the AChE structure. Usually, simulations are utterly dependent on crystallography to provide initial structures. In this case, the 2 techniques were employed synergistically, the simulations helping to provide and verify details of the protein structure that were not apparent from X-ray crystallography alone. This is an important step beyond the well-established role for molecular dynamics simulation in crystallographic structure refinement.

In view of the ease with which large quaternary ammonium ligands diffused into the active site of the crystalline protein (Harel et al., 1993), it was somewhat surprising to find that the opening of the active site gorge was tightly blocked in the crystal. Moreover, the gorge was too narrow in its static dimensions to allow these ligands or ACh to penetrate into the active site. These observations forced us to consider the potential for conformational change in the gorge walls and the possibility that alternative routes to the active site exist. In particular, we aimed to determine whether movement or penetration of a relatively thin portion of the gorge wall, comprised of residues 67-94, was likely or even possible. Part of this wall, near Trp 84, is only 1 atom thick and is a plausible candidate for a "back door" to the active site (Ripoll et al., 1993). Furthermore, the segment comprising this thin wall is homologous to a loop which blocks the active site of *G. candidum* lipase. This lipase has a very similar overall fold to AChE (Cygler et al., 1993), as well as to human lipase, in which it has been shown that this loop serves as a movable "lid" on the active site (Lawson et al., 1992; van Tilbeurgh et al., 1993).

Although our initial simulation was initiated for the purpose of illuminating potential conformational changes, we nonetheless doubted its validity because the simulated structure quickly deviated from the crystal structure in only 1 localized region, and this region included the active site. In an attempt to reconcile these discrepancies, the all-hydrogen parameter force field used in the CHARMM simulation was adapted for use in X-PLOR and the structure was re-refined. These parameters appeared to have no effect and can only be interpreted as being unrelated to the discrepancy.

In further efforts to reconcile these discrepancies, we reexamined the electron density map from which the 1ACE structure was derived and prepared a new map that incorporated low-resolution data. The latter map was an important key to discovering that DECA was present in the "native" structure. In the map prepared using only high-resolution data, the density in this region had been previously interpreted as a string of 5 water molecules. The inclusion of DECA in our simulations did not lead to any clear improvement in the overall agreement between the simulation and the crystal structure (Fig. 6A; Kinemage 2); neither did it help to maintain the active site triad near the X-ray structure (Fig. 6B; Kinemage 2).

Finally, notice was taken of the crystallization conditions used and of the possibility that peaks ascribed to water might actually be NH_4^+ ions, since the mother liquor giving rise to the AChE crystals was equilibrated with a solution of 61% saturated $(NH_4)_2SO_4$. We found that substitution of NH_4^+ ions for 2 water peaks near the bottom of the gorge resulted in a remarkable improvement in the agreement between the ensemble of structures generated by the molecular dynamics and the X-ray structure (Fig. 6B; Kinemage 2).

Thus, the simulations prompted a reexamination of the crystal structure and provided a useful test of the hypothesis that DECA was present. The simulations cannot prove the presence of 2 NH_4^+ ions in this structure nor can they distinguish between NH_4^+ and Na^+ ions. However, the concentration of NH_4^+ in the crystallization liquor (>4 M) is at least 10-fold greater than that of Na^+, and the enhanced agreement between simulation and crystal structure is highly suggestive of their presence. Additional evidence to support or refute these findings is being sought through attempts to crystallize AChE that had never been exposed to DECA and by the use of NH_4^+-free buffers.

Due to the complexity of the simulated system, it is difficult to ascertain how the presence of 2 cations can have such a dra-

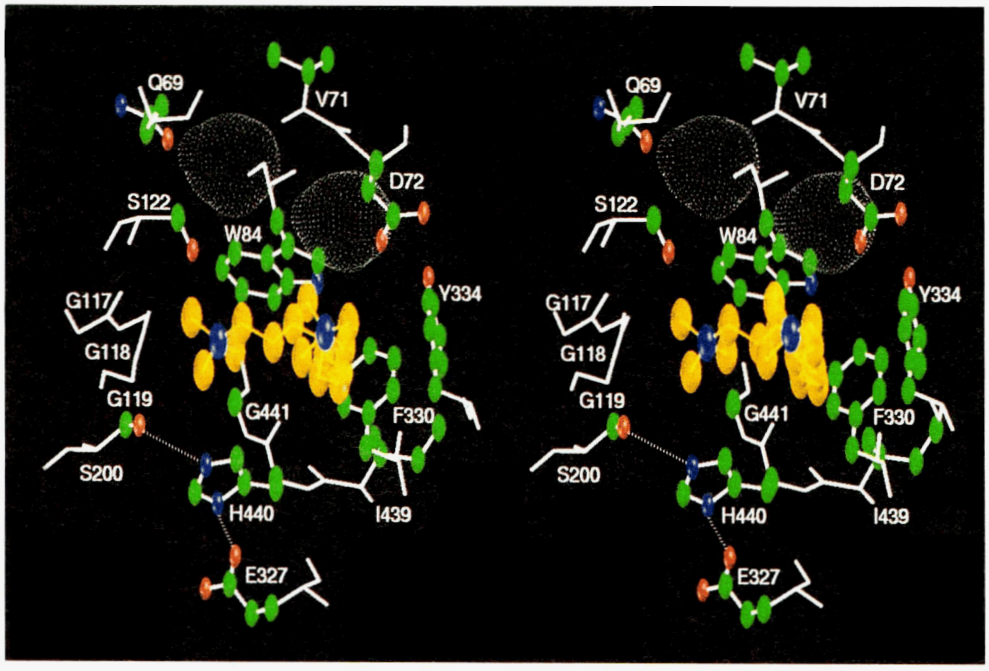

Fig. 7. The position of 2 ammonium ions relative to DECA and protein residues in the region of the active site. The unlabeled molecule in the center is DECA (yellow); the dot surfaces represent the VDW surfaces of 2 ammonium ions (white). When waters substitute for the ions, or when their charges are neutralized, there are changes in the average conformation of Gln 69 and clockwise around to Gly 441, with the largest deviations from the crystal structure occurring in His 440 and Gly 441. Image generated using RIBBONS by M. Carson.

matic effect on the stability of the side chains of the active site triad and of residues 82–85. Molecular dynamics simulations behave chaotically, obscuring ordinary cause-and-effect relationships. This is especially problematic here because there is no direct contact between the putative ions and the active site triad (Fig. 7). The DECA molecule is interposed between them and may serve to mediate the interaction between these ions and the triad residues. However, one must assume that DECA is not unique in this ability, since the active site configuration is similar when edrophonium or tacrine substitutes for DECA (Harel et al., 1993). Simulations conducted in the absence of DECA, but with cations at peaks 1 and 2, deviate to an even greater extent than do those without cations in the gorge (data not shown). It will be of interest, therefore, to examine a crystal structure of AChE in the absence of any ligands.

We considered the possibility that the difference between simulations obtained by the insertion of cations might be a random occurrence. We thought it worthwhile, therefore, to rerun the simulations with either different random number seeds or, in our case, on another computer that applies slightly different arithmetic standards. The trajectories run on the 2 machines, namely an SGI 4D/440 and a Cray YMP, exhibit nearly the same RMS deviation between each other as they do relative to the crystal structure, yet the relationship of the presence of the 2 cations and the active site conformation is maintained. Furthermore, this relationship is lost when the charge on the cations is neutralized either at the beginning or after 10 ps of simulation.

Our simulations were conducted with all histidines assigned neutral charges and with only water in the protein exterior. The former condition may be unrealistic for the crystalline protein, and the latter certainly is. However, the behavior of the gorge may be quite different out of the crystalline environment, and it may be of considerable value to adopt biological solvent conditions (e.g., no blocking of the gorge), both expecting and allowing the simulation to depart from the crystal structure. Whether attempting to study the crystalline protein or the protein in solution, however, any detailed analysis of electrostatic forces within the gorge of the 1ACE structure must take into account the apparent requirement for conformational change in the gorge wall as ligands approach the active site and the high probability that small cations are present in the gorge.

Since DECA is a bis-quaternary cation, we have reconciled our simulation to the crystal structure by, in essence, adding 3 positive charges at the base of the gorge and 1 positive charge at the top. The charge at the top does not appear to be crucial for structural integrity, since structures containing single molecules of edrophonium and tacrine are virtually identical to the structure containing DECA (Harel et al., 1993). Moreover, these other structures indicate that the shape of the gorge is not determined by the DECA ion. The forces stabilizing the conformation of residues forming the gorge wall are not immediately evident, but it is clear that they are to some extent indifferent to the particular ligand that is present.

We find it remarkable that DECA remains in the gorge after several days of dialysis of the soluble protein prior to crystallization, yet is gone a few days after the crystalline protein has been exposed to another suitable ligand. This suggests that the release of DECA from the AChE gorge must be triggered by another ligand, although in solution DECA acts as a reversible inhibitor with an inhibition constant (K_i) of 0.034 μM, in 0.01 M Tris, pH 7.6, for the *Torpedo* AChE preparation used for crystallization (Eichler et al., 1994). It should be noted, however, that the K_i for DECA is ionic strength-dependent (Berman & Decker, 1986). The persistence of DECA in the AChE gorge may be a peculiar consequence of the conditions employed, but it is clear in any case that the cationic ligands edrophonium and tacrine were sufficient (in the crystal), and NH_4^+ and Na^+ were not sufficient (either in solution or in the crystal), to induce the release of DECA from AChE. It is intriguing to speculate on whether the cationic natural substrate, ACh^+, and/or the reac-

tion product, choline, may participate in such a mechanism, and whether this phenomenon somehow reflects the manner in which AChE was designed to respond to its substrate.

The putative cation-binding sites that we have identified in this work are near the bottom of the active site gorge, at a point where the gorge is relatively wide. Assuming that the crystal structure is retained under physiological conditions, there appears to be sufficient space in this region of the gorge for ACh^+ or $choline^+$ to occupy these sites. We do not yet understand the movement of substrate and products through this area, but it is plausible that these cation-binding sites may be functionally important in the catalytic process. A hint regarding the mechanism and direction of product release may be provided by our observation that the insertion of a third small cation at peak 3 induces a conformational change and the penetration of a cation at peak 2 through the gorge wall. Alternatively, Trp 84 undergoes an in-plane rotation and displacement ("shutter-like") to various degrees in all of our simulations and may thereby provide access to the active site (Gilson et al., 1994).

In summary, our results underscore the need to understand the effect of crystallization conditions on crystal structure and to take into account the possibility that simulations that deviate from an initial X-ray structure may actually point to an incorrectly refined or incomplete structure. They also point to the merit of including low-resolution data when producing electron density maps, even if these data were not used for refinement. The ability to reconcile the simulation and the crystal structure to the degree now reported leaves us in a position of greater confidence in the validity of AChE simulations that deviate from the crystal structure when modifications are made to the protein, the ligands, or the solvent.

Methods

All crystallographic refinements were performed using X-PLOR (Brünger et al., 1987) as described previously (Sussman et al., 1991). Because the unit cells had slightly different dimensions for the various data sets listed in Table 1, and to avoid any bias in the maps examined, a uniform X-PLOR protocol was used for all the data sets, starting from the 1ACE coordinates (including only the protein atom coordinates). This protocol included: (1) rigid body refinement, (2) positional refinement, (3) slow cooling (to 2,000 K), (4) positional refinement, and (5) individual *B*-factor refinement. After this "preliminary" refinement on all $F_o > 0\sigma$ (6–2.8 Å resolution), $F_o - F_c$ difference Fourier maps were calculated based on all $F_o > 0\sigma$ (20–2.8 Å resolution). All simulations were performed using the molecular dynamics simulation program CHARMM (Brooks et al., 1983), and starting coordinates were taken from entry 1ACE in the Brookhaven Protein Data Bank (Bernstein et al., 1977; Sussman et al., 1991). We used an all-hydrogen model and parameter set (MacKerell et al., 1992) because there is an abundance of aromatic residues lining the gorge, and prior experience has demonstrated the inability of models employing only polar hydrogens (i.e., united or extended atom models) to faithfully represent the dynamics of such residues (Axelsen et al., 1991). A 25-Å stochastic boundary (Berkowitz & McCammon, 1982; Brünger et al., 1984; Brooks et al., 1985) with a 2-Å buffer region was centered on atom C_α of Gly 77 based upon the following consideration: allowing for a 2-Å buffer zone of harmonically constrained atoms, residues in the active site triad, all residues comprising the gorge, and residues from a symmetry-related copy that block the gorge orifice (see Results) are within 23 Å of the origin and thus free to move unconstrained within the boundary. Furthermore, the number of atoms within this boundary represents a tractable computational problem (see below), and the boundary conveniently excludes residues 1–3, 485–489, and 535–537, which were not seen in the 2.8-Å 1ACE structure. The coordinates for several side chain atoms within the boundary were also not seen; these were generated through CHARMM, using idealized internal coordinates.

The unoccupied space within the boundary was filled with 3-atom water models (TIP3P; Jorgensen et al., 1983), as described previously (Axelsen et al., 1988). A shifted 12-Å cutoff and a dielectric constant of 1.0 were used for nonbonded interactions. All acidic and basic residues were given unit electrostatic charges; all histidine residues were neutral. The outermost 2-Å shell of atoms was coupled to a 300 K temperature bath, and all non-hydrogen atoms in this shell were harmonically constrained according to their crystallographic temperature factors, as described previously (Axelsen & Prendergast, 1989). Bonds to hydrogen atoms were constrained with SHAKE (Ryckaert et al., 1977). All protein segments throughout the simulation system were covalently linked to at least 1 residue in the shell. The simulation was propagated with a Verlet algorithm and a step size of 1.0 fs. Following 100 steps of adapted-basis Newton–Raphson (ABNR) minimization, the system was assigned random velocities appropriate for a system at 300 K and propagated without velocity rescaling. Temperature equilibration was achieved within 10 ps, but since we cannot predict the rate at which other features of the simulation will equilibrate (Axelsen & Prendergast, 1989), we do not designate a specific interval as the equilibration period. There were 3,897 atoms in the primary molecule (out of 8,132 total in AChE), 1,920 atoms in the symmetry-related copy, and 798 TIP3P water molecules, for a total of 8,211 atoms. On a Cray YMP, the simulation required 6.7 h of CPU time and 29.9 Mw of memory to progress 10 ps.

Acknowledgments

This study was supported by U.S. Army Medical Research and Development contract DAMD17-93-C-3070, l'Association Franco-Israeliénne pour la Recherche Scientifique et Technologique (AFIRST), the Minerva Foundation, and the Kimmelman Center for Biomolecular Structure and Assembly. Use of the Cray YMP supercomputers was supported by the Minnesota Supercomputer Institute and the National Cancer Institute–Frederick Cancer Research Facility. I.S. is Bernstein-Mason Professor of Neurochemistry. P.H.A. is a Markey Scholar in Biomedical Science and is supported by the Markey Charitable Trust. We thank Carlos Faerman, Michael Gilson, J. Andrew McCammon, Mia Raves, Daniel Ripoll, and Giuseppi Zaccai for stimulating discussions; Christian Cambillau and Art Chirino for the TOM program; Boaz Shaanan and Gil Shoham for help in X-ray data collection on the R-Axis Image Plate System at the Hebrew University, Jerusalem; and Leon Esterman for computational support.

References

Axelsen PH, Gratton E, Prendergast FG. 1991. Experimentally verifying molecular dynamics simulations through fluorescence anisotropy measurements. *Biochemistry 30*:1173–1179.

Axelsen PH, Haydock C, Prendergast FG. 1988. Molecular dynamics of tryptophan in ribonuclease-T1 I. Simulation strategies and fluorescence anisotropy decay. *Biophys J 54*:249–258.

Axelsen PH, Prendergast FG. 1989. Molecular dynamics of tryptophan in ribonuclease-T1 II. Correlations with fluorescence. *Biophys J 56*:43–66.

Berkowitz M, McCammon JA. 1982. Molecular dynamics with stochastic boundary conditions. *Chem Phys Lett 90*:215–217.

Berman HA, Decker MM. 1986. Kinetic, equilibrium, and spectroscopic studies on dealkylation ("aging") of alkyl organophosphonyl acetylcholinesterase. *J Biol Chem 261*:10646–10652.

Bernstein FC, Koetzle TF, Williams GJB, Meyer EF Jr, Brice MD, Rodgers JR, Kennard O, Shimanouchi T, Tasumi M. 1977. The Protein Data Bank: A computer-based archival file for macromolecular structures. *J Mol Biol 112*:535–542.

Brooks BR, Bruccoleri RE, Olafson BD, States DJ, Swaminathan S, Karplus M. 1983. CHARMM: A program for macromolecular energy, minimization, and dynamics calculations. *J Comp Chem 4*:187–217.

Brooks CL III, Brünger A, Karplus M. 1985. Active site dynamics in protein molecules: A stochastic boundary molecular-dynamics approach. *Biopolymers 24*:843–865.

Brünger AT. 1990. *X-PLOR, a system for crystallography and NMR, manual version 3.1*. New Haven, Connecticut: Yale University Press.

Brünger AT, Brooks CL III, Karplus M. 1984. Stochastic boundary conditions for molecular dynamics simulations of ST2 water. *Chem Phys Lett 105*:495–500.

Brünger AT, Kuriyan J, Karplus M. 1987. Crystallographic *R* factor refinement by molecular dynamics. *Science 235*:458–460.

Connolly ML. 1983. Solvent-accessible surfaces of proteins and nucleic acids. *Science 221*:709–713.

Cygler M, Schrag JD, Sussman JL, Silman I, Gentry MK, Doctor BP. 1993. Relationship between sequence conservation and three-dimensional structure in a large family of esterases, lipases, and related proteins. *Protein Sci 2*:366–382.

Eichler J, Anselmet A, Sussman JL, Massoulié, Silman I. 1994. Differential effects of 'peripheral' site ligands on *Torpedo* and chicken acetylcholinesterase. *Mol Pharmacol 45*:335–340.

Gilson MK, Straatsma TP, McCammon JA, Ripoll DR, Faerman CH, Axelsen PH, Silman I, Sussman JL. 1994. Open "back door" in a molecular dynamics simulation of acetylcholinesterase. *Science*. Forthcoming.

Harel M, Schalk I, Ehret-Sabatier L, Bouet F, Goeldner M, Hirth C, Axelsen P, Silman I, Sussman JL. 1993. Quaternary ligand binding to aromatic residues in the active-site gorge of acetylcholinesterase. *Proc Natl Acad Sci USA 90*:9031–9035.

Jorgensen WL, Chandrasekhar J, Madura JD, Impey RW, Klein ML. 1983. Comparison of simple potential functions for simulating liquid water. *J Chem Phys 79*:926–935.

Lawson DM, Brzozowski AM, Dodson GG. 1992. Lifting the lid of lipases. *Curr Biol 2*:473–475.

Lee BK, Richards FM. 1971. The interpretation of protein structures: Estimation of static accessibility. *J Mol Biol 55*:379–400.

Leszczynski JF, Rose GD. 1986. Loops in globular proteins: A novel category of secondary structure. *Science 234*:849–855.

MacKerell AD Jr, Bashford D, Bellott M, Dunbrack RL Jr, Field MJ, Fischer S, Gao J, Guo H, Ha S, Joseph D, Kuchnir L, Kuczera K, Lau FTK, Mattos C, Michnick S, Nguyen DT, Ngo T, Prodhom B, Roux B, Schlenkrich M, Smith J, Stote R, Straub J, Wiorkiewicz-Kuczera J, Karplus M. 1992. Self-consistent parameterization of biomolecules for molecular modeling and condensed phase simulations. *Biophys J 61*:A143. [Abstr]

Nachmansohn D, Wilson IB. 1951. The enzymic hydrolysis and synthesis of acetylcholine. *Adv Enzymol 12*:259–339.

Quinn DM. 1987. Acetylcholinesterase: Enzyme structure, reaction dynamics, and virtual transition states. *Chem Rev 87*:955–975.

Ringe D, Petsko GA. 1985. Mapping protein dynamics by X-ray diffraction. *Progr Biophys Mol Biol 45*:197–235.

Ripoll DR, Faerman CH, Axelsen PH, Silman I, Sussman JL. 1993. An electrostatic mechanism for substrate guidance down the aromatic gorge of acetylcholinesterase. *Proc Natl Acad Sci USA 90*:5128–5132.

Ryckaert JP, Ciccotti G, Berendsen HJC. 1977. Numerical integration of the Cartesian equations of motion of a system with constraints: Molecular dynamics of *n*-alkanes. *J Comput Phys 23*:327–341.

Sussman JL, Harel M, Frolow F, Oefner C, Goldman A, Toker L, Silman I. 1991. Atomic structure of acetylcholinesterase from *Torpedo californica*: A prototypic acetylcholine-binding protein. *Science 253*:872–879.

Sussman JL, Harel M, Frolow F, Varon L, Toker L, Futerman AH, Silman I. 1988. Purification and crystallization of a dimeric form of acetylcholinesterase from *Torpedo californica* subsequent to solubilization with phosphatidylinositol-specific phospholipase C. *J Mol Biol 203*:821–823.

Sussman JL, Silman I. 1992. Acetylcholinesterase: Structure and use as a model for specific cation–protein interactions. *Curr Opin Struct Biol 2*:721–729.

Tan RC, Truong TN, McCammon JA, Sussman JL. 1993. Acetylcholinesterase: Electrostatic steering increases the rate of ligand binding. *Biochemistry 32*:401–403.

van Tilbeurgh H, Egloff M-P, Martinez C, Rugani N, Verger R, Cambillau C. 1993. Interfacial activation of the lipase–procolipase complex by mixed micelles revealed by X-ray crystallography. *Nature 362*:814–820.

Weise C, Kreienkamp HJ, Raba R, Pedak A, Aaviksaar A, Hucho F. 1990. Anionic subsites of the acetylcholinesterase from *Torpedo californica*: Affinity labelling with the cationic reagent *N,N*-dimethyl-2-phenylaziridinium. *EMBO J 9*:3885–3888.